Computation & theory

Microstructure simulation of AA2219 alloy in hot/warm forming and heat treatment using cellular automata methods

Tao Zhang[1,2] , Junwen Chen[1,2], Hai Gong[1,2,*], Yunxin Wu[1,2], Tiewen Hao[1,2,3], and Xiaofeng He[4]

[1] *Light Alloy Research Institute, Central South University, Changsha 410083, China*
[2] *State Key Laboratory of Precision Manufacturing for Extreme Service Performance, Central South University, Changsha 410083, China*
[3] *Dalian Engineering Technology Co., LTD, China First Heavy Industries, Dalian 116600, China*
[4] *Zhejiang Junhong Machinery Co., LTD, Lishui 323000, China*

ABSTRACT

The preparation of component with 2219 aluminum alloy consists of hot/warm forming and the subsequent heat treatment, inducing complex microstructure evolution. The microstructure simulation in forming and solution treatments is investigated using cellular automata (CA) models, consisting of initial microstructure generation model, static recrystallization (SRX) model and thermal–mechanical treatment model. The effect of parameters (temperature, strain, strain rate and pass interval time) on the microstructure characteristic is analyzed. SRX occurs during the pass interval time by the transformation from low-angle grain boundaries into high-angle grain boundaries. Low temperature, large strain and strain rate during the hot compression contribute to the SRX process during pass interval time due to the resulted higher dislocation. Warm forming is beneficial for the increased dislocation density and sub-grain structures, which change to equiaxed grains after solution treatment, indicating the total recrystallization. The increased strain and strain rate, and lower temperature in the warm forming process contribute to the grain refinement and acceleration of the velocity of the SRX process after solution treatment. Experiments of hot compression, warm compression followed by solution treatment are conducted. The CA simulated flow stress and microstructure agree with the experimental results. The CA models established can provide guidance for the microstructure evolution for the hot/warm forming and the subsequent heat treatment of aluminum alloy.

Address correspondence to E-mail: gonghai@csu.edu.cn

Introduction

2219 aluminum alloy (AA2219) has been widely used in the aerospace industry due to its advantages of high strength, good weldability and ductility at low temperatures [1, 2], such as transition ring and tank of the rocket [3, 4]. The preparation of AA2219 components mainly consists of hot forming, warm forming and the subsequent heat treatment. Its mechanical properties and its anisotropy depend on the microstructure during the forming and heat treatments [5].

The microstructure evolution during the multipass forming and the heat treatment is quite complex. The microstructure analysis methods, such as metallographic test, electron back scatter diffraction (EBSD), scanning electron microscopy (SEM) or transmission electron microscopy (TEM), can be only used to characterize the microstructure at specified positions or forming stage of the material. The microstructure evolution during the multi-pass forming and its distribution at different positions are difficult to be acquired. Microstructure simulation methods have been developed to have a better understanding of the microstructure evolution during the complex forming and heat treatment processes, such as phase field (PF) models [6–8], Monte Carlo (MC) models [9, 10], cellular automata (CA) models [11–13] and molecular dynamics models [14, 15]. The complex issues of the microstructure transformation and evolution can be adopted with CA models, and the differential equations of physical metallurgy can be described by discrete element method and randomized algorithms. Therefore, the grain deformation and the recrystallization of the material during forming and heat treatment are investigated using CA models in this study.

CA models had been used to simulate the microstructure variation induced by dynamic recrystallization (DRX) [16], meta-dynamic recrystallization (MDRX) [17], static recrystallization (SRX) [18] and the thermo-mechanical treatment (TMT) process [19]. During the one-pass forming process, dynamic nucleation and its growth are the main mechanism. Zhang [16] studied the DRX behavior of copper by CA simulation during hot compression. DRX kinetics model based on the modified Avrami equation was proposed to describe the DRX behavior. The grain topology changed during the

forming process. To describe the effect of deformation on grain topology more accurately, Chen [20] established an updated topology deformation technique, in which a cellular coordinate system and a material coordinate system were established separately. Bakhtiari [21] studied the reconstruction of deformed microstructure and changes in the microstructure in mesoscale. Accordingly, the normal growth, topology deformation, and reconstruction of texture and grain boundary misorientation techniques were used to reconstruct the deformed microstructure. Timoshenkov [22] studied the microstructure evolution in a C-Mn micro-alloyed steel using CA during thermo-mechanical treatment. The developed probabilistic-based model integrated the effects of the individual metallurgical phenomena related to the hot rolling process, such as hot deformation, DRX and precipitation state, where the retarding effect of precipitates was considered. Jin [23, 24] proposed a new approach to identify the nucleation parameter during DRX, and adaptive response surface method was applied as optimization model to provide input parameters to CA model. Madej [25] established the fully coupled random CA and finite element (FE) model for simulation of a DRX progress. The FE solver provided information on equivalent stress, equivalent strain, and temperature fields as well as on geometry of deformed computational domain after each time step. These data were transferred to the developed random CA model, which was responsible for evaluation of corresponding microstructure morphology evolution and dislocation density changed under DRX conditions. Finally, a set of data from the random CA part was send back to the FE solver and used as an input for the next time step.

The static softening is the main mechanism in the pass interval time during the multi-pass forming process [26, 27], and previously published studies showed that the flow stress and microstructure both changed in the pass interval time for aluminum alloy [28, 29]. Zhang [30] investigated the SRX behavior of Ni-based superalloy through CA model and provided insight into the factors affecting the SRX microstructure evolution significantly involving the time step, size of cell, nucleation location and orientation of nucleation. Lin [18] developed a CA model with probabilistic state switches to simulate the microstructural evolution during SRX, and the kinetics of SRX was formulated on a mesoscale level. Sitko

[31] developed a parallel version of a complex, physics-based CA-SRX model, which significantly increased the computational efficiency. Zheng [32] established a physically based CA model and integrated the effects of the individual metallurgical phenomena related with the steel strip hot rolling, including hot deformation, SRX, meta-dynamic recrystallization (MDRX) and DRX. It provided a link of multi-scale modeling to bridge the macroscopic thermo-mechanical parameters and the mesoscopic microstructure. Zhang [33] proposed a coupled CA-FEM to simulate the microstructure evolution of multi-pass hot rolling process and predicted the average grain size of the rolled plate resulting from the combination of DRX, MDRX and SRX.

Thermo-mechanical treatment [33, 34] was considered to refine the grains and improve the mechanical properties of the material. The increased dislocations in the deformation process contributed to the precipitation of the strengthening phases during the subsequent heat treatment. Yu [35] established CA model of stainless steel during TMT process, and the results showed the microstructure evolution of the recrystallization under different conditions and exhibited the changes of precipitation along with the deformation. Zheng [36] investigated the concurrent ferrite recrystallization and austenitic transformation during intercritical annealing of cold-rolled dual-phase steel by CA modeling. The simulations provided insight into the microstructural phenomena that resulted from the interaction of primary recrystallization and phase transformation. Salehi [11] proposed a coupled CA-FEM to evaluate SRX kinetics during non-isothermal annealing of cold deformed low carbon steels. The effects of various factors including heating rate, annealing temperature and initial microstructures had been considered in the model to accurately predict the SRX kinetics and the final microstructures. Madej [37] established a multi-scale model of microstructure evolution during cold rolling and the subsequent annealing of a two-phase ferritic–pearlitic sample. The digital material representation taking into account exact representation of the microstructure morphology was used in the research to investigate inhomogeneous strain distribution during cold rolling and the SRX behavior during the annealing treatment.

Many previously published articles had analyzed the microstructure variation induced by DRX or heat treatment. However, the preparation of AA2219 consists of hot forming, warm forming and the followed heat treatment, and the previous forming process will affect the microstructure characteristics, thus significantly changing the microstructure condition in the followed treatment. Additionally, the key parameters forming and heat treatment play vital role in the microstructure evolution. For example, large 2219 Al alloy rings used to connect propellant tank components of a satellite launch vehicle to each other were conventionally manufactured by radial–axial hot ring rolling, which resulted in coarse elongated grain and low ductility. He [38, 39] proposed an improved process and a product with fine and uniform grains as well as significant increase in elongation can be acquired, including hot ring rolling, warm ring rolling followed by heat treatment. Therefore, in this study, CA models of AA2219 during the hot/warm forming and solution treatments are established and the effects of parameters (temperature, strain, strain rate and pass interval time) on the microstructure characteristic are analyzed. Experiments of hot compression, warm compression followed by solution treatment are conducted for validation of CA models.

Cellular automaton models

The preparation of component with 2219 aluminum alloy mainly consists of hot forming, warm forming and the subsequent heat treatment. The temperature in hot forming is higher than the recrystallization temperature and large deformation can be achieved in this process. As a result, coarse grains and large secondary particles formed in the casting process can be effectively refined. Warm forming is beneficial for the accumulation of the deformation energy, which contributes to the dispersive distribution of the strengthening phases and strengths enhancement during the subsequent heat treatment. Additionally, there will be less grain growth in the warm forming process due to its lower forming temperature compared to that in the hot forming process.

Microstructure evolution mechanism

For the multi-pass deformation and the subsequent heat treatment processes, complex mechanism for the microstructure evolution will take place. For the AA2219, work hardening (WH), dynamic recovery

(DR) and continuous dynamic recrystallization (CDRX) occur during the deformation process. The dislocation density inside the material significantly increases with the increased strain, and the tangled dislocation appears during the WH process. The material reaches the thermodynamic instability due to the internal free energy, and the dislocation density will decrease at high temperature through the movements of slip, climbing and cross slip; as a result, dislocation cell forms and it gradually changes to sub-grains with low-angle grain boundaries (LAGBs) during the DR process. With the proceeding of the deformation process, the sub-grains start to migrate by absorbing the dislocation and then transform into high-angle grain boundaries (HAGBs), which is the CDRX. Static recovery (SR), meta-dynamic recrystallization (MDRX) and static recrystallization (SRX) take place during the pass interval time and the subsequent heat treatment. The accumulated dislocation density in the deformation process decreases during the pass interval time by the dislocation annihilation induced by the migration of the sub-grains in SR process. The free energy at grain interfaces decreases during the pass interval time, and the sub-grain boundaries migrate under the driving force to achieve the growth of sub-grains in SRX process. Different to the conventional solution and artificial aging treatment, the thermal–mechanical treatment (TMT) consists of the deformation process and the subsequent heat treatment. The deformation energy accumulated in the deformation process will contribute to the formation of the sub-grains and its growth during the subsequent heat treatment. Therefore, the microstructure simulation of the thermal–mechanical treatment includes the initial microstructure generation, SRX models and TMT models.

The physical metallurgy behavior of metal alloy always was described with differential equations. Solving these differential equations was time-consuming, and it may also cannot get solutions of these equations for complex object. However, the complex object is divided into cells discrete in time and space in CA model, and complex issues can be described through random algorithm and transition rules between the cell and its neighborhood. The random algorithm was known to be effective in describing the microstructure evolution as the microstructure variation shows the characteristics of randomness. The transition rules can be applied between the cell and

its neighborhood, such as the nucleation and grain growth of recrystallization process. Status values of each cell are updated at each time step according to the transition rules. Therefore, CA models established in this study were adopted to describe the DRX, SRX and TMT behavior, and the relationship between flow stress and microstructure was analyzed.

Initial microstructure generation

To simulate the SR and SRX behavior during the multi-pass interval time, the initial microstructure is the final deformed structure. The CA model of CDRX was described in author's previously published article [40]. Estrin–Mecking models [40] are adopted to describe the variation in dislocation density, as shown in Eqs (1)–(3). The relationship between the flow stress under different forming parameters and the dislocation density is shown in Eq. (4).

$$d\rho/d\varepsilon = k_1 - k_2\rho \tag{1}$$

$$k_1 = 1/bl \tag{2}$$

$$k_1 = k_2(\sigma_s/\alpha Gb)^2 \tag{3}$$

$$\sigma = \alpha Gb\sqrt{\rho} \tag{4}$$

where ρ is the dislocation density, ε is the true strain, k_1 and k_2 are the work hardening coefficients of work hardening and dynamic softening, respectively. b is the Burger vector, l is the mean free path of dislocation, σ_s is the steady flow stress, α is the material constant, G is the shear modulus.

Model of SRX

The dislocation annihilation related to the pass interval time [28] due to the SR process is shown in Eq. (5). The initial value of the dislocation density for the SR process is the dislocation immediately after the deformation process, and it will decrease to the value without any strain with sufficient pass interval time, as shown in Eq. (6).

$$d\rho/dt = -k_s(\rho - \rho_0)^n \tag{5}$$

$$\rho = \begin{cases} \rho_d & (t = 0) \\ \rho_0 & (t = \infty) \end{cases} \tag{6}$$

where ρ is the dislocation density, ρ_d is the dislocation density immediately after the deformation, ρ_0 is the dislocation density without any strain, t is the

pass interval time, k_s and n are the coefficient and exponent of SR, respectively.

The coefficient of SR is related to the holding temperature during the pass interval time and it increases with the increased temperature [41], as shown in Eq. (7). Additionally, the value of the exponent of SR varies under different deformation conditions. According to Eq. (5), the dislocation density for the SR process can be described in Eq. (8) for $n \neq 1$ at low temperature and Eq. (9) for $n = 1$ at high temperature. Based on Yoshie's analysis [42], the value of n was set as 1 in the case of annihilation of dislocations at lattice defects like grain boundaries by climbing of dislocations, while it was 2 in the case of annihilation by coalescence of dislocations pairs.

$$k_s = k_0 d_0^{m_s} \exp(-Q_s/RT) \tag{7}$$

$$\rho = \left[(\rho_d - \rho_0)^{1-n} + (n-1)k_s t \right]^{1/1-n} \quad (n \neq 1) \tag{8}$$

$$\rho = (\rho_d - \rho_0) \exp(-k_s t) + \rho_0 \quad (n = 1) \tag{9}$$

SRX consists of the nucleation of recrystallized nuclei and its growth, and the nucleation is related to the growth of the sub-grains. The pre-deformation can induce the formation of fine sub-grains, and the high temperature is beneficial for the growth of the sub-grains. The sub-grains will transform into the recrystallized nuclei, and the deformation energy accumulated in the deformation process contributes to the nucleation. The nucleation rate in SRX process was related to the temperature and the strain rate during the deformation process, according to Guo's model [43], as shown in Eq. (10). The size of the nuclei is quite small, and it is difficult to be qualitatively investigated using the microstructure analysis methods. The nucleation rate can be obtained based on the stress–strain curves and metallographic structure of the static recrystallized grains according to Ding's results [44], as shown in Eq. (11).

$$\dot{n} = C \dot{\varepsilon}^m \exp\left(-\frac{Q_n}{RT} \right) \tag{10}$$

$$X_s = \dot{n} \frac{\varepsilon}{\dot{\varepsilon}} \frac{4}{3} \pi D_s^3 \tag{11}$$

where C is the material constant, m is the sensitivity coefficient of strain rate, Q_n is active energy and R is the mole gas constant, ε is the true strain, X_s is the SRX fraction, D_s is the mean size of static recrystallized grain.

There is significant difference of the dislocation density between the deformed grains and the recrystallized grains. The dislocation density of the deformed grains increases with the proceeding of the deformation process, while it decreases to the initial value without any strain for the recrystallized grains. Additionally, the deformation energy accumulated in the deformation process contributes to the growth of the recrystallized grains. The velocity of the grain boundaries (GBs) movement was related to the GBs mobility and the pressure exerted on the GBs, as shown in Eqs. (12–13). The GBs moves along the normal direction of the local GBs with a certain velocity.

$$v = Mp \tag{12}$$

$$M = \frac{\delta D_{0b} b}{kT} \exp\left(-\frac{Q_b}{RT} \right) \tag{13}$$

where v is the migration velocity, M is the mobility of the grain boundary, p is the pressure, δ is the characteristic thickness of grain boundary, D_{0b} is the boundary self-diffusion coefficient, k is Boltzmann constant and Q_b is the diffusion activation energy of grain boundary.

The driving force for the grains growth is related to the variations in the energy during the grains growth process, including the consumed volume energy and the new generated surface energy. The volume energy is related to the dislocation density difference between adjacent grains, while the surface energy is determined by the misorientation angle difference between adjacent grains, as shown in Eqs. (14–16). Read–Shockley equation was used to describe the GBs energy for different grains; nevertheless, it was only suitable for the grains with small misorientation angle. A modified Read–Shockley relationship was adopted to describe the relationship between the GBs energy and the misorientation angle, as shown in Eqs. (17–18). Additionally, the secondary precipitated phase of Al$_2$Cu is the main strengthening phase for 2219 aluminum alloy, which plays a pinning effect on the migration of the GBs. A pinning coefficient of β on the GBs migration was considered and it was related to the deformation temperature and the strain rate, as shown in Eqs. (19–20).

$$F = \frac{dW}{dr} = 4\pi r^2 \tau \Delta\rho - 8\pi r \gamma \tag{14}$$

$$\Delta\rho = \rho_d - \rho_0 \tag{15}$$

$$p = \frac{F}{4\pi r^2} = \tau\Delta\rho - \frac{2\gamma}{r} \tag{16}$$

$$\gamma = \gamma_m \sin(2\theta)\{1 - r_\gamma \ln[\sin(2\theta)]\} \, 0 \le \theta \le 90° \tag{17}$$

$$\gamma_m = Gb\theta_m/4\pi(1 - \lambda) \tag{18}$$

$$v = \beta Mp \tag{19}$$

$$\beta = A_\beta \, \dot{\bar{\varepsilon}}^{n_\beta} \exp\left(-\frac{Q_\beta}{RT}\right) \tag{20}$$

where F is the driving force, r is the grain radius, τ is the dislocation line energy, $\triangle\rho$ is the dislocation density difference between the recrystallized grain and the deformed grain, γ is the GB energy, γ_m is the GB energy of high angle boundary, θ is the misorientation angle between the ith recrystallized grain and its neighboring grain, θ_m is the critical misorientation angle, λ is Poisson's ratio.

The deformation will significantly change the microstructure morphology as the grains will be compressed through the compression direction and elongated vertical to the compression direction. The fraction and the length of the GBs are the key factor for the migration of the GBs during the grain growth process due to its high deformation energy compared to that of the grain interiors. Therefore, the grain topology model was adopted and the effect of true strain on the variation in the grain topology was considered to improve the simulation accuracy, as shown in Eq. (21).

$$\begin{pmatrix} m_x \\ m_y \end{pmatrix} = \begin{pmatrix} l_{xx} & 0 \\ 0 & l_{yy} \end{pmatrix} \begin{pmatrix} u_x \\ u_y \end{pmatrix} \tag{21}$$

where u_x and u_y are cell size in horizontal and vertical directions before deformation, m_x and m_y are cell size after each CA steps with deformation, ε is true strain and the relationship between ε and l is $\ln l_i = \varepsilon_i$.

Model of TMT

The accumulated deformation energy is beneficial for the nucleation and the subsequent grain growth during the solution treatment. During the TMT process, the recrystallized grains start to nuclear in a rate ($\dot{n}_s$) for SRX after meeting the requirements for the nucleation of SRX, as shown in Eq. (22). The deformation energy is proportional to the dislocation density; meanwhile, the dislocation density can be described using the flow stress, as shown in Eqs. (23–24).

$$\dot{n}_s = \alpha_0(E - E_c)\exp\left(\frac{-Q_N}{RT_s}\right) \tag{22}$$

$$E = cG\rho b^2 \tag{23}$$

$$E = c\sigma^2/\alpha^2 G \tag{24}$$

where E is the deformation energy, E_c is the critical deformation energy for SRX, Q_N is the thermal activation energy of nucleation, T_s is the solution temperature and it is set as 813 K in this study, c is the material constant.

Results output

(1) SRX fraction

The SRX fraction can be calculated by the ratio of the number of static recrystallized cells to the total cells in the simulated zone, as shown in Eq. (25).

$$X_s = N_s/N \tag{25}$$

where X_s is SRX fraction, N_s is the number of static recrystallized cells and N is total number cells in simulation.

(2) Average dislocation density

The SRX fraction can be calculated by the ratio of the number of static recrystallized cells to the total

$$\bar{\rho} = \sum_1^n \rho_i/n \tag{26}$$

where $\bar{\rho}$ is the average dislocation density, ρ_i is the dislocation density for each cell, n is the number of the total cells.

(3) Simulated flow stress

The SRX fraction can be calculated by the ratio of the number of static recrystallized cells to the total

$$\sigma_{CA} = \alpha Gb\sqrt{\bar{\rho}} \tag{27}$$

where σ_{CA} is the simulated flow stress using CA method.

Experiments

As discussed in Sect. "Microstructure evolution mechanism" section, the preparation of component with 2219 aluminum alloy consists of hot forming, warm forming and the subsequent heat treatment.

The forming parameters, such as the temperature, strain, strain rate and pass interval time, play a vital role in the microstructure evolution of 2219 aluminum alloy during multi-pass forming process. First, two-pass hot compression was conducted and the effects of forming parameters on the microstructure evolution during the pass interval time were investigated. The material of the hot compression was forged 2219 aluminum alloy, and it was machined into the cylinder with a diameter of 10 mm and a height of 15 mm. The material was heated to the hot compression temperature (623 K, 723 K, 773 K) with a heating rate of 5 K/s and a holding time of 3 min. A reduction in the height direction (20%, 30%, 40%) was applied with different strain rates (0.1 s^{-1}, 1 s^{-1}, 10 s^{-1}), and different pass interval time (5 s, 30 s, 60 s) was applied to the specimens under the hot compression temperature. The second pass compression was then conducted with the same temperature and strain rate of the first pass with different reduction. The total reduction in the two passes was 60%.

For the warm forming process, one pass compression was conducted at different temperatures (473 K, 523 K, 573 K), reductions (20%, 30%, 40%) and strain rates (0.1 s^{-1}, 1 s^{-1}, 5 s^{-1}). It should be noted that the true strain for different pass reduction (20%, 30%, 40%) was 0.22, 0.36 and 0.51. The solution treatment was applied to the warm compressed specimen with the temperature of 813 K and a holding time of 4 h, which is the TMT process. Table 1 shows the parameters of the hot and warm compression experiments.

The specimens were quenched immediately after the compression or the solution treatment to reserve the microstructure. They were ground and electrolytic polished with the voltage of 20 V and polishing time of 50 s. The grain morphology was observed by the EBSD experiments.

Results and discussion

Hot compression

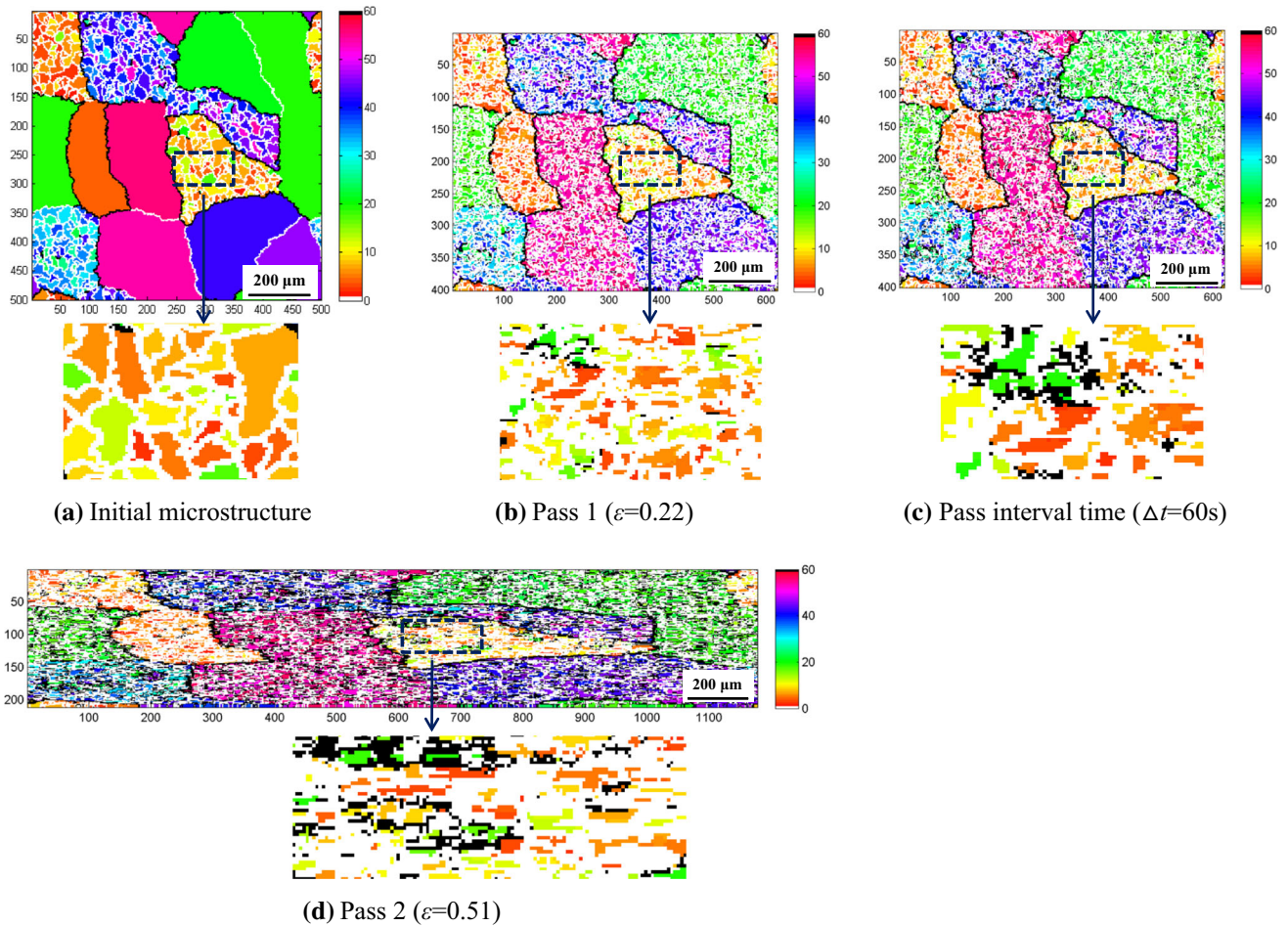#### Microstructure evolution in two-pass hot compression

Figure 1 shows the microstructure evolution during the two-pass hot compression. It should be noted that the initial microstructure is the forged structure followed by solution treatment, which consists of the deformed grains and the substructure with dominant low-angle grain boundaries (LAGBs). A large number of sub-grains appear in the grains interiors accompanied by the generation of high-angle grain boundaries (HAGBs), indicating that CDRX is triggered in the first pass compression. There is no obvious change of grain morphology during the pass interval time, while the fraction of HAGBs is significantly increased resulting from the SRX process, as shown in Fig. 1b. It can be inferred that the fraction of SRX is small due to no obvious change of grain morphology. As a result, there will be SR and SRX induced by the migration of the sub-grain boundaries. The grains are severely elongated during the second pass compression, and the fraction of HAGBs is further increased. The accumulated strain during two-pass hot compression contributes to the CDRX process.
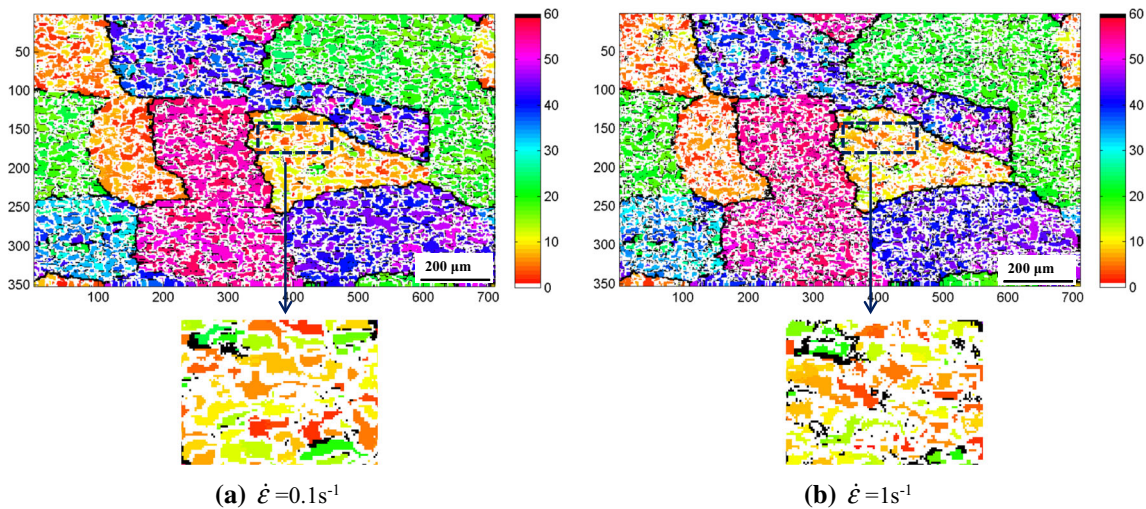
Effect of parameters on microstructure variation

The strain rate during the first pass of the hot compression has little effect on the change of grain morphology, as shown in Fig. 2. The fraction of sub-grain boundaries significantly increases with the increased

Table 1 Parameters of hot and warm compression

Treatment	Parameter	Value
Two-pass hot compression	Temperature/T	623 K, 723 K, 773 K
	Strain rate/$\dot{\varepsilon}$	0.1 s^{-1}, 1 s^{-1}, 10 s^{-1}
	True strain per pass/ε	0.22, 0.36, 0.51
	Pass interval time/$\triangle t$	5 s, 30 s, 60 s
One-pass warm compression	Temperature/T	473 K, 523 K, 573 K
	Strain rate/$\dot{\varepsilon}$	0.1 s^{-1}, 1 s^{-1}, 5 s^{-1}
	True strain per pass/ε	0.22, 0.36, 0.51
Solution treatment	Temperature/T	813 K

(a) Initial microstructure   **(b)** Pass 1 (ε=0.22)   **(c)** Pass interval time ($\triangle t$=60s)

(d) Pass 2 (ε=0.51)

Figure 1 Variation in microstructure during two-pass hot compression (T = 623 K, $\dot{\varepsilon}$ = 0.1 s^{-1}).

(a) $\dot{\varepsilon}$ =0.1s^{-1} **(b)** $\dot{\varepsilon}$ =1s^{-1}

Figure 2 Effect of strain rate on microstructure variation during pass interval time (T = 723 K, ε = 0.36, $\triangle t$ = 60 s).

strain rate; meanwhile, SRX occurs during the pass interval time resulting from the increased fraction of HAGBs. Large amounts of dislocation and finer sub-grains can be generated under higher strain rate during the first pass of the hot compression. The accumulated deformation energy of the sub-grains

provides the driving force for the migration of the LAGBs during the pass interval time, which contributes to the accumulation of the LAGBs and its transformation into HAGBs. The fraction of HAGBs increases from 18.4% to 21.8% with the increase in the strain rate from 0.1 to 1 s^{-1}, as shown in Table 2.The dislocation density will be decreased obviously during the SRX process, and the extent of the transformation from LAGBs into HAGBs can be used to describe the fraction of the SRX process.

Figure 3 shows the effect of temperature on the microstructure during the pass interval time. The grain morphology does not change at different temperature, while the fraction of sub-grain boundaries decreases with the increased temperature. Higher temperature in the first pass compression will decrease the dislocation density inside the material due to its slip, climbing and cross slip in the DR process. The dislocation rearrangement and annihilation can be achieved by the slip for the dislocations in the same slip system, climbing and cross slip for that in different slip systems. The stacking fault energy plays a vital role in the evolution of the dislocation at high temperature. The movement of the dislocation is more likely to occur for 2219 aluminum alloy at high temperature due to its higher stacking fault energy compared to other metals. Therefore, the deformation energy and the fraction of sub-grain boundaries both decrease at high temperature. Additionally, high temperature and small strain rate are beneficial for the CDRX in the hot compression process, which promotes the transformation from LAGBs to HAGBs with the depletion of the deformation energy. As a result, there is no sufficient energy for the migration of the LAGBs during the pass interval time. It is known that the high temperature can increase the kinetic energy of the atoms and accelerate the migration of the sub-grain boundaries, which may contribute to the recrystallization process. However, decreased deformation energy at high temperature plays a dominant role in the weakening the SRX process due to the decreased fraction of HAGBs with the increased temperature during the pass interval time, as shown in Table 3. The average misorientation also decreases with the increase in temperature, indicating that higher temperature in the first pass compression will impede the SRX process in the subsequent pass interval time.

The strain rate during the first pass of the hot compression has little effect on the change of grain morphology, as shown in Fig. 2. The fraction of sub-grain boundaries significantly increases with the increased strain rate; meanwhile, SRX occurs during the pass interval time resulting from the increased fraction of HAGBs. Large amounts of dislocation and finer sub-grains can be generated under higher strain rate during the first pass of the hot compression. The accumulated deformation energy of the sub-grains provides the driving force for the migration of the LAGBs during the pass interval time, which contributes to the accumulation of the LAGBs and its transformation into HAGBs. The fraction of HAGBs increases from 18.4 to 21.8% with the increase in the strain rate from 0.1 to 1 s^{-1}, as shown in Table 2.The dislocation density will be decreased obviously during the SRX process, and the extent of the transformation from LAGBs into HAGBs can be used to describe the fraction of the SRX process. As a result, the average misorientation decreases from 9.6° to 9.2° with the increased strain rate.

As shown in Table 4, the fraction of HAGBs increases with the increased strain during the first pass of the hot compression. The dislocation density inside the material increases during the first pass deformation, which contributes to the migration of the GBs and the transformation from LAGBs into HAGBs. The accumulated deformation energy in the first pass compression provides the driving force for the recrystallization process during the pass interval time; as a result, the average misorientation increases.

The temperature and dislocation density both change during the pass interval time, which will obviously affect the SRX process, as discussed in Sect. "Model of SRX" section. It can be seen from Table 5 that the pass interval time has positive effect on the transformation from LAGBs into HAGBs. The accumulated deformation energy and temperature during the first pass contribute to the migration of the GBs and the formation of HAGBs. The pass interval time is beneficial for the accumulation of the HAGBs, which will trigger SRX process.

Table 2 Effect of strain rate on microstructure parameters (T = 723 K, ε = 0.36, $\triangle t$ = 60 s)

Parameter	$\dot{\varepsilon}$ = 1 s^{-1}	$\dot{\varepsilon}$ = 0.1 s^{-1}
Fraction of HAGBs/η_{HAGB}	21.8%	18.4%
Average misorientation/θ_m	9.6°	9.2°

(a) *T* = 623 K   **(b)** *T* = 723 K   **(c)** *T* = 773 K
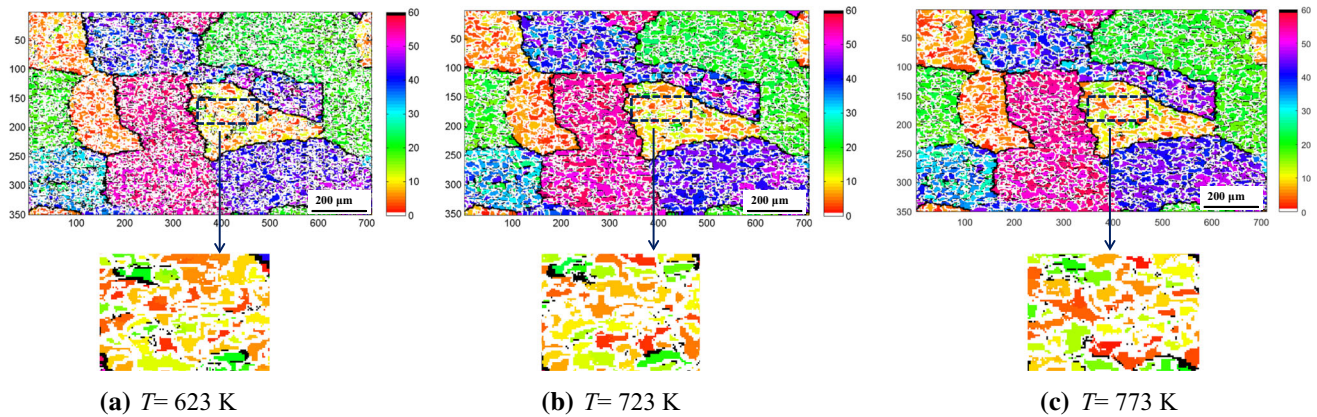
Figure 3 Effect of temperature on microstructure variation during pass interval time ($\dot{\varepsilon} = 0.1$ s^{-1}, $\varepsilon = 0.36$, $\triangle t = 60$ s).

Table 3 Effect of temperature on microstructure parameters ($\dot{\varepsilon} = 0.1$ s^{-1}, $\varepsilon = 0.36$, $\triangle t = 60$ s)

Parameter	$T = 623$ K	$T = 723$ K	$T = 773$ K
Fraction of HAGBs/η_{HAGB}	23.1%	21.8%	21.3%
Average misorientation/θ_m	11.5°	9.6°	8.1°

Table 4 Effect of strain on microstructure parameters ($\dot{\varepsilon} = 0.1$ s^{-1}, $T = 723$ K, $\triangle t = 60$ s)

| Parameter	$\varepsilon = 0.22$	$\varepsilon = 0.36$	$\varepsilon = 0.51$
Fraction of HAGBs/η_{HAGB}	18.7%	21.8%	27.3%
Average misorientation/θ_m	8.5°	9.6°	10.9°

Table 5 Effect of pass interval time on microstructure parameters ($\dot{\varepsilon} = 0.1$ s^{-1}, $\varepsilon = 0.36$, $T = 623$ K)

Parameter	$\triangle t = 5$ s	$\triangle t = 30$ s	$\triangle t = 60$ s
Fraction of HAGBs/η_{HAGB}	12.4%	18.7%	22.8%
Average misorientation/θ_m	8.02°	8.4°	8.6°

Figure 4 shows the effect of parameters on the fraction of SRX during the pass interval time. It can be seen that the value of SRX fraction is smaller than 25%, indicating the insufficient SRX process for the AA2219. The SR plays a primary role in the pass interval time due to the high stacking fault of AA2219. The dislocation density decreases due to the SR process with the climbing of dislocations and the coalescence of dislocations pairs. The decreased dislocation density cannot provide sufficient driving force for the migration of the sub-grain boundaries and its transformation into the HAGBs.

The increased pass interval time is beneficial for the transformation from LAGBs into HAGBs, which contributes to the SRX process. Additionally, AA2219 is strengthened by the precipitation of secondary phase particles (Al$_2$Cu). There is growth of the secondary phase particles with the increased pass interval time, which may decrease the strengthening effect and contribute to the SRX process. The SRX fraction decreases from 21.3 to 7.7% with the temperature increasing from 623 to 773 K. The dislocation density significantly decreases under high temperature; nevertheless, the dislocation movement and the sub-grain boundaries migration are more likely to occur with high temperature. Furthermore, high temperature is beneficial for the dissolution of the secondary phase particles, while its size will also increase, promoting the static softening effect. As a result, it can be concluded from Fig. 4a that the decrease in dislocation and the growth of secondary phase particles play a significant role at higher temperature, thus decreasing the SRX fraction. The dislocation density is obviously accumulated under large strain rate, resulting in large deformation energy. Meanwhile, there is not sufficient time for the growth of the secondary phase particles during deformation stage, which will be grown up during the pass interval time. The accumulated deformation
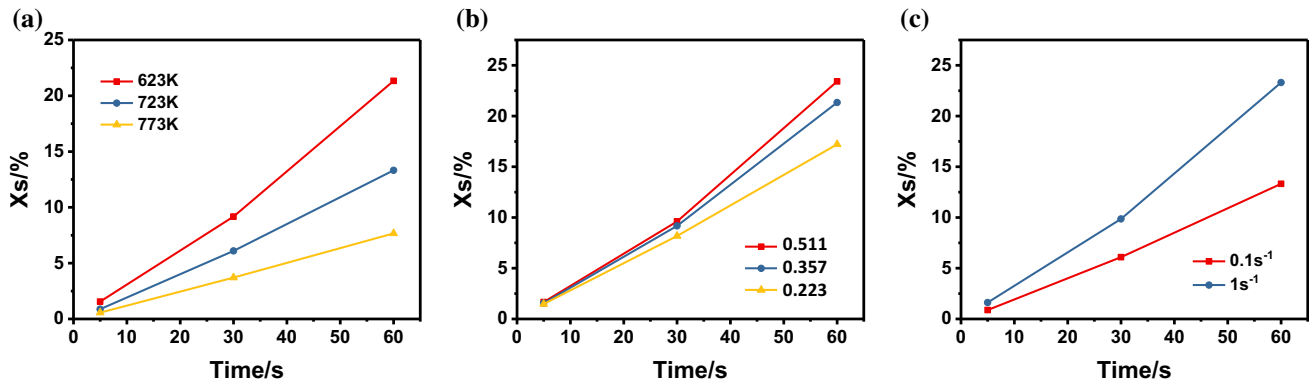
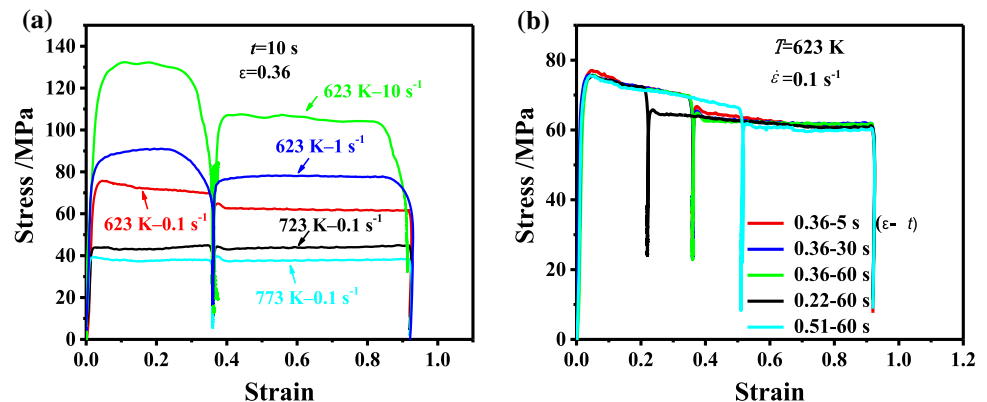**Figure 4** Effect of: **a** temperature; **b** strain; **c** strain rate on the fraction of SRX.

energy and the decreased strengthening effect induced from the large secondary phase particles both promote the SRX process, as shown in Fig. 4b. The increased strain contributes to the transformation from LAGBs into HAGBs; as a result, the SRX fraction increases from 17.2 to 23.4%.

Experiment verification

Figure 5 shows the strain–stress curves under different parameters during two-pass hot compression. There is a significant drop of the flow stress during the second pass, resulting from the static softening effect during the pass interval. It can be seen that the static softening effect increases with low temperature, large strain rate and long pass interval time, which is consistent with the variation in SRX fraction discussed in Sect. "Effect of parameters on microstructure variation" section. The static softening effect mainly consists of SR and SRX, which can be described with Eq. (28).

$$X_s = (F_s - 0.2)/(1 - 0.2) \tag{28}$$

where X_s is the SRX fraction and F_s is the static softening fraction.

Figure 6 shows the comparisons of simulated results and experimental values of SRX fraction and flow stress. The simulated flow stress is related to the dislocation density inside the material and can be calculated by Eq. (28). The SRX fraction and flow stress agree with the experimental results.

Thermo-mechanical treatment

Microstructure evolution in thermo-mechanical treatment

Figure 7 shows the variation in microstructure during the warm compression and the followed solution treatment. It should be noted that the initial microstructure for the warm compression process is the hot compressed structure, which consists of the elongated grains with large sub-grain structure. The number of sub-grains increases significantly during the warm compression process, as shown in Fig. 7b. The migration of sub-grains is limited at low temperature of the warm compression, which is

Figure 5 Effect of: **a** temperature and strain rate; **b** strain and pass interval time on the flow stress.

Figure 6 Comparisons of simulated results and experimental values of: **a** SRX fraction; **b** flow stress.
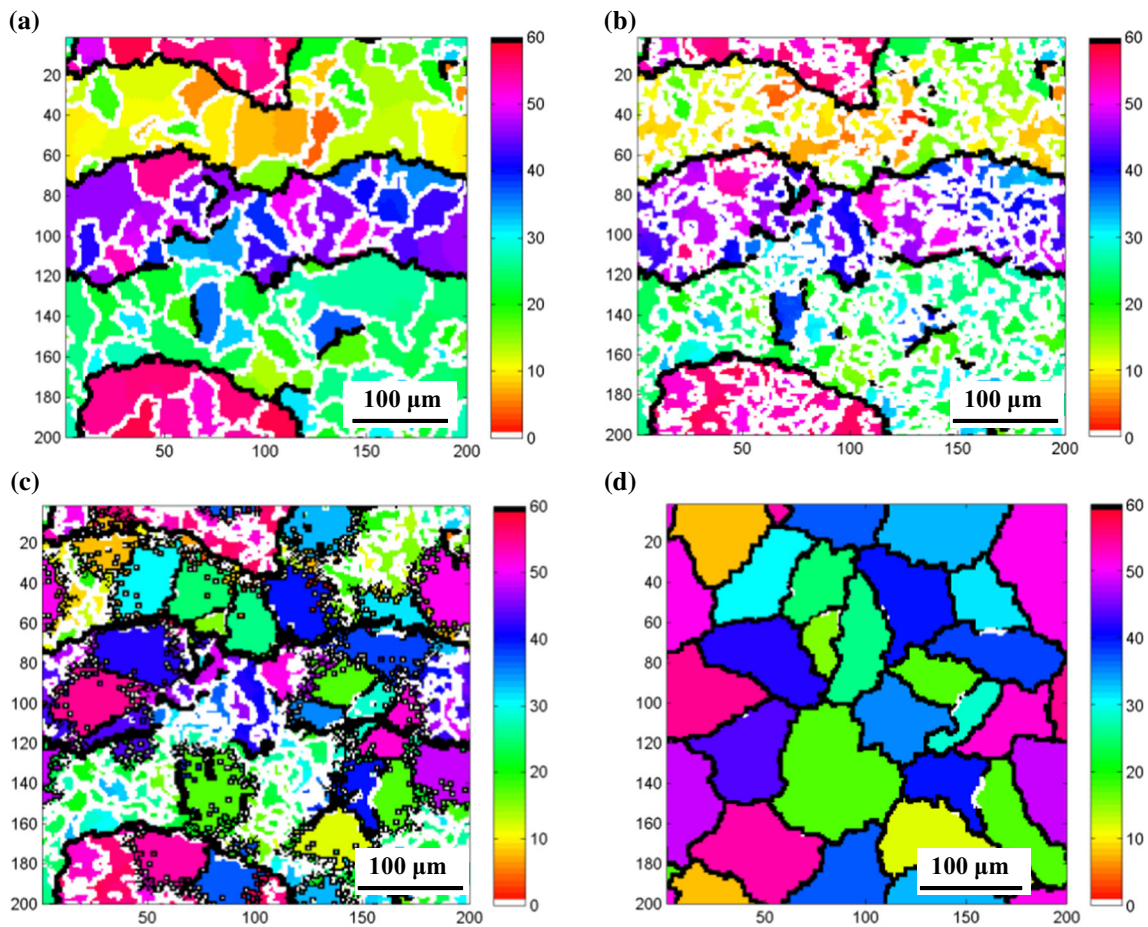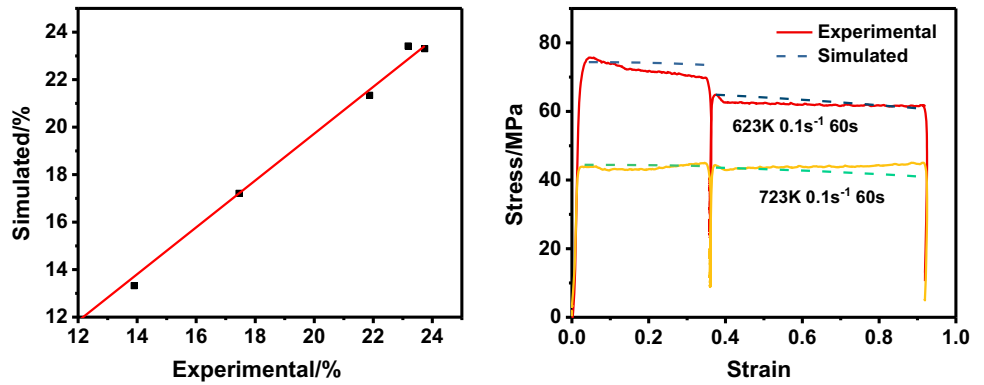
Figure 7 Variation in microstructure during thermo-mechanical treatment: **a** Before warm compression; **b** after warm compression ($T = 573$ K, $\varepsilon = 0.9$, $\dot{\varepsilon} = 0.01$ s^{-1}); **c** with recrystallized fraction of 50%; **d** with recrystallized fraction of 100%.

beneficial for the accumulation of the dislocation density and the deformation energy inside the material, resulting in an unstable state with high energy of the material. During the followed solution treatment, high surface energy of the sub-grain boundaries contributes to the migration and nucleation of the sub-grain boundaries. Then, the sub-grain boundaries will gradually transform to HAGBs with accumulation of misorientation, which is the recrystallization process. It can be seen large number of nuclei appear at the sub-grain boundaries with depletion of its surface energy. Finally, all the sub-grain boundaries change to equiaxed grains with the proceeding of the solution time; as a result, total

recrystallization occurs, as shown in Fig. 7d. The warm compression process contributes to the increase in surface energy and the number of sub-grains, which provides the driving force for the migration at high temperature during the solution treatment. The migrated sub-grains will absorb the dislocation density during the migration process and then change to HAGBs; therefore, the average dislocation density and deformation energy both decrease.

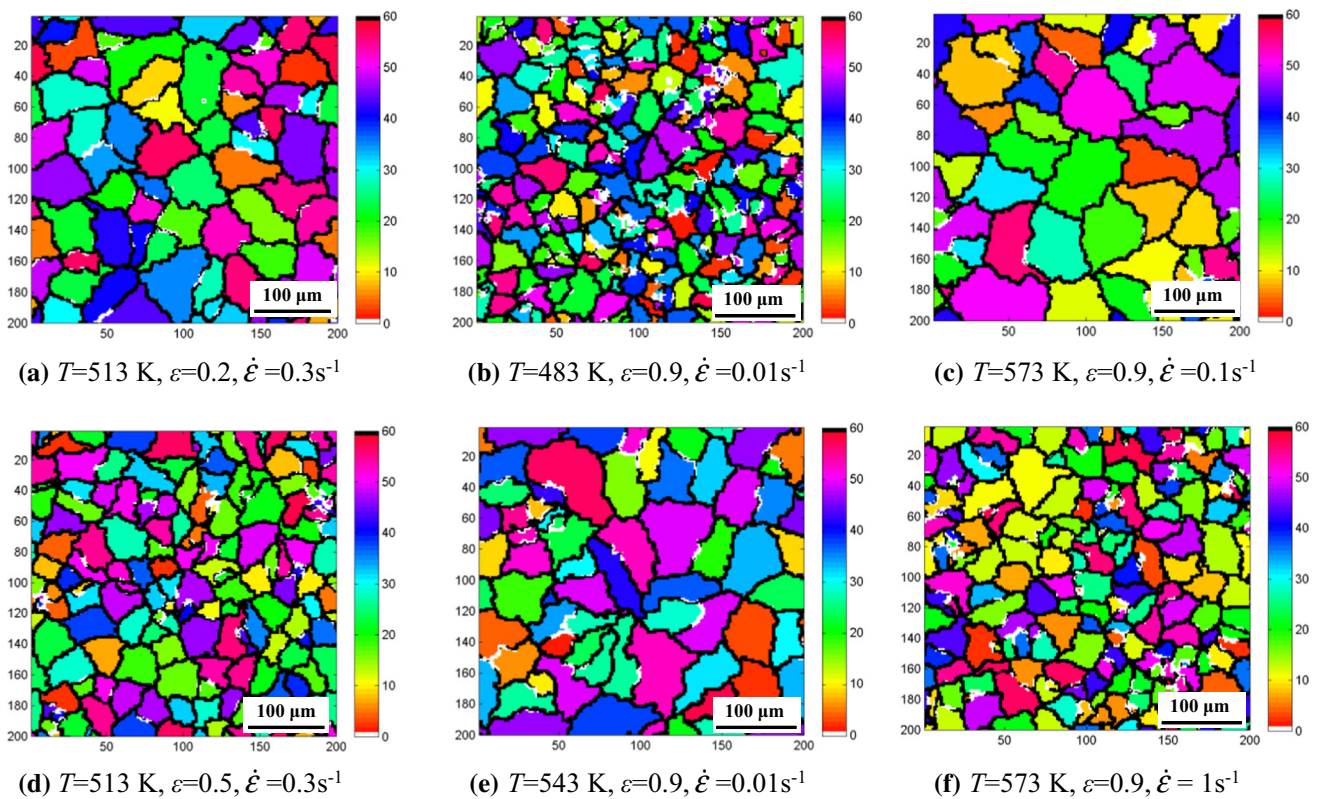## Effect of parameters on microstructure variation

Figures 8, 9 show the microstructure and average grain size after solution treatment with different forming parameters. It can be seen that total recrystallization occurs for all the samples with different forming parameters during the solution treatment. Nevertheless, the forming parameters significantly affect the effect of the grain refinement, which is related to the deformation energy accumulated in the forming process.

The average grain size decreases from 56.4 to 29.5 μm with the increased strain ranging from 0.2 to 0.9, as shown in Fig. 8a, d. The dislocation density
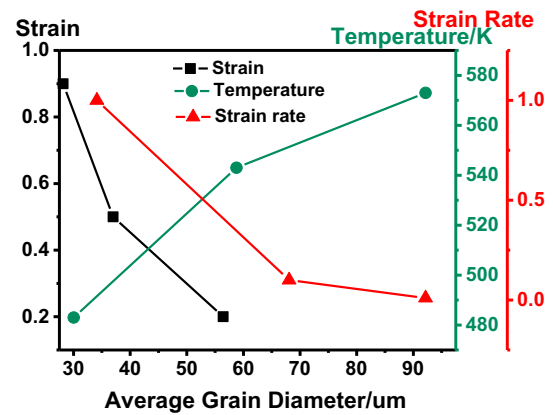
Figure 9 Average grain size after solution treatment with different forming parameters.

and misorientation increase with the increased strain during the warm forming process; meanwhile, the static nucleation rate also increases during the solution treatment. More static nuclei will result in smaller grain size and higher SRX rate. The average grain size significantly increases with the increased temperature during the warm forming process. High temperature is beneficial for the DR process, which will decrease the dislocation density and the

(a) T=513 K, ε=0.2, $\dot{\varepsilon}$ =0.3s^{-1}

(b) T=483 K, ε=0.9, $\dot{\varepsilon}$ =0.01s^{-1}

(c) T=573 K, ε=0.9, $\dot{\varepsilon}$ =0.1s^{-1}

(d) T=513 K, ε=0.5, $\dot{\varepsilon}$ =0.3s^{-1}

(e) T=543 K, ε=0.9, $\dot{\varepsilon}$ =0.01s^{-1}

(f) T=573 K, ε=0.9, $\dot{\varepsilon}$ = 1s^{-1}

Figure 8 Microstructure after solution treatment with different forming parameters.

deformation energy of the material. Additionally, high temperature leads to the growth of the sub-grains and decreased number of the sub-grains. There is negative correlation between the static nucleation rate and the temperature in warm forming process. Therefore, grain growth at higher deformation temperature obviously occurs during the solution treatment. The average grain size decreases from 92.2 to 34.1 μm with the increased strain rate, indicating that large strain rate contributes to the grain refinement, as shown in Fig. 8c, f. Pilling up of the dislocations is generated under large strain rate during the forming process, and there is insufficient time for the recovery of the dislocations; as a result, deformation energy of the material is increased and a large number of fine sub-grain structures are generated. Large strain rate plays a positive role in the nucleation rate and the numerous fine sub-grain structures providing driving force for the SRX process and the grain refinement.

As shown in Fig. 10, large strain and strain rate in the forming process both accelerate the velocity of the SRX process as the accumulated deformation energy and sub-grain structures will decrease the incubation period before the SRX process. Nevertheless, large strain and strain rate both result in lower SRX fraction even though they contribute to the grain refinement. Higher temperature decreases the velocity of the SRX process due to the dislocation annihilation and sufficient DR process under high deformation temperature.

Experiment verification

Figure 11 shows the EBSD results after solution treatment with different forming parameters. Total

recrystallized microstructure with no preferential grain orientation is generated under solution treatment, and no deformed grains can be seen. The solution treatment provides the energy for the atomic diffusion and the sub-grains migration, and the elongated or compressed grains induced by the forming process will be replaced by new generated equiaxed grains.
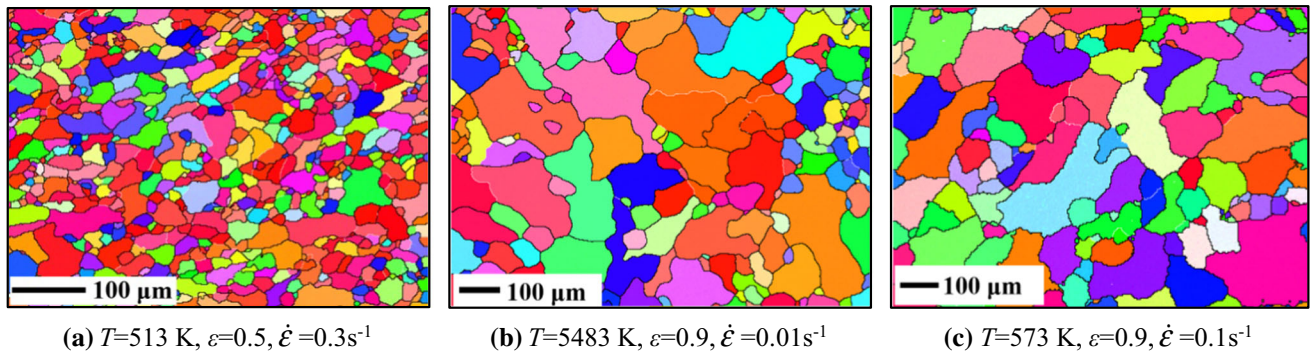
Table 6 shows the comparisons of simulated and experimental average grain size, which is consistent with the variation described in Fig. 9. The CA simulated results agree with the experiments with a fitting coefficient of 0.997, as shown in Fig. 12. The maximum error of the average grain size is 11.11%. The CA models established in this study can provide guidance for the microstructure evolution in the forming and the followed heat treatment.

Conclusions

(1) The microstructure evolution mechanism of AA2219 in multi-pass deformation and the subsequent heat treatment processes is revealed, consisting of WH, DR, CDRX and SRX processes. CA models are established to simulate the microstructure evolution.

(2) CDRX will be triggered in the hot compression through the transformation from LAGBs into HAGBs. SRX process occurs during the pass interval time with the increased fraction of HAGBs.

(3) Low temperature, large strain and strain rate during the hot compression as well as long pass interval time contribute to the SRX process during pass interval time. The HAGBs fraction and average misorientation both increase under
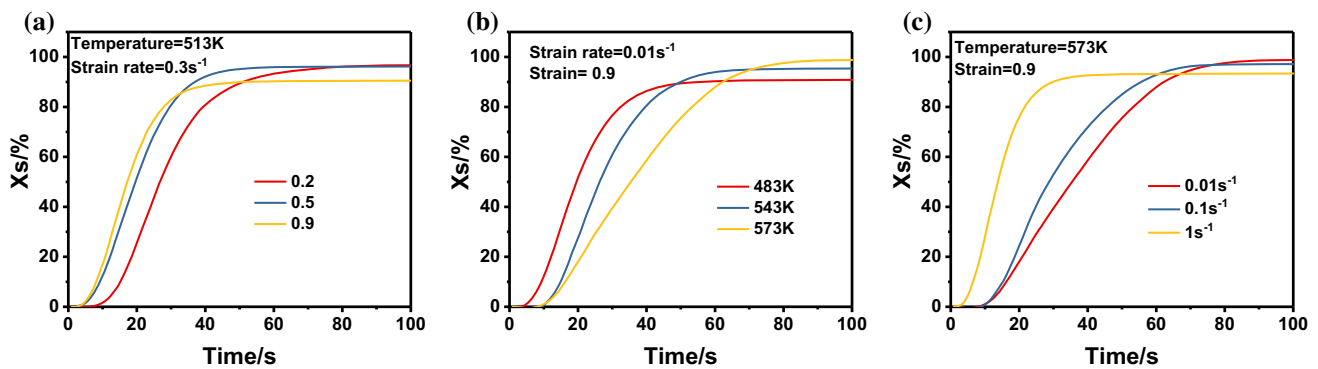

Figure 10 Effect of: **a** strain; **b** temperature; **c** strain rate on the fraction of SRX.

(a) T=513 K, ε=0.5, $\dot{\varepsilon}$ =0.3s^{-1} **(b)** T=5483 K, ε=0.9, $\dot{\varepsilon}$ =0.01s^{-1} **(c)** T=573 K, ε=0.9, $\dot{\varepsilon}$ =0.1s^{-1}

Figure 11 Experimental microstructure after solution treatment with different forming parameters.

Table 6 Comparisons of simulated and experimental average grain size after solution treatment

Parameters		Average grain size/μm		
		Experiment	CA simulation	Error/%
T = 513 K, $\dot{\varepsilon}$ = 0.3 s^{-1}	ε = 0.2	60	56.4	6.00
	ε = 0.5	35	37.0	5.71
	ε = 0.9	33	29.5	10.61
$\dot{\varepsilon}$ = 0.01 s^{-1}, ε = 0.9	T = 483 K	27	30.0	11.11
	T = 543 K	58	58.8	1.38
	T = 573 K	87	92.2	5.98
T = 573 K, ε = 0.9	$\dot{\varepsilon}$ = 0.01 s^{-1}	87	92.2	5.98
	$\dot{\varepsilon}$ = 0.1 s^{-1}	65	68.1	4.77
	$\dot{\varepsilon}$ = 1 s^{-1}	32	34.1	6.56
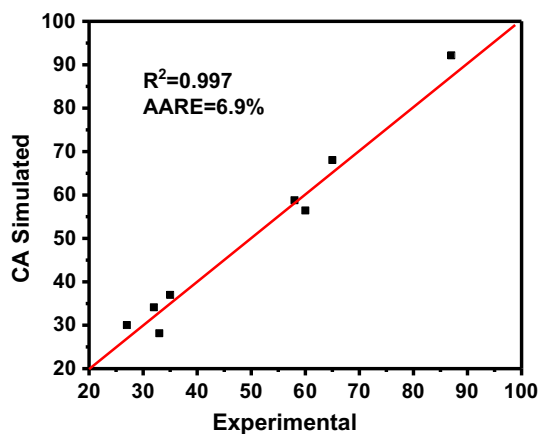
Figure 12 Comparisons of simulated results and experimental values.

these parameters, resulting in increased SRX fraction.

(4) Compared to hot forming, the dislocations and the number of sub-grain structures increase in warm forming due to the low forming temperature and weak dislocation annihilation induced by recovery process. The accumulated dislocations and the number of sub-grain structures both contribute to the recrystallization and grain refinement.

(5) Total recrystallization occurs during the solution treatment for the samples with different forming parameters. Large strain and strain rate, and low temperature in the warm forming process contribute to the grain refinement and acceleration of the velocity of the SRX process after solution treatment.

Acknowledgements

Author contribution

TZ involved in conceptualization, writing—original draft, resources, data curation. JC took part in writing, methodology, and editing. HG involved in supervision and project administration. YW involved in funding acquisition. TH involved in visualization, validation, formal analysis.

Data availability

Due to the nature of this research, participants of this study did not agree for their data to be shared publicly, so supporting data are not available.

Declarations

Conflict of interest The authors declare that they have no known competing financial interests or personal relationships that could have appeared to influence the work reported in this paper.

Ethical approval Ethics Committee approval was obtained from the Institutional Ethics Committee of Central South University to the commencement of the study. This manuscript did not involve human tissue.

References

[1] Cheng M, Luo G, Xiao X, Song L (2022) Microstructure evolution of pulsed laser melting 2219 aluminum alloy: solidification modes and inter-pulse thermal cycles. Mater Lett 313:131768

[2] Wan Z, Wang Q, Zhao Y, Zhao T, Shan J, Meng D, Song J, Wu A, Wang G (2022) Improvement in tensile properties of 2219–T8 aluminum alloy TIG welding joint by PMZ local properties and stress distribution. Mat Sci Eng A-Struct 839:142863

[3] Zhu H, Huang L, Wang Z, Li J, Ma H, Su H (2019) Fracture behaviour of laser-welded 2219–T6 aluminium alloy under pulsed Lorentz force. J Mater Sci 54:9857–9874. https://doi.org/10.1007/s10853-019-03588-4

[4] Roh A, Um HY, Kim D, Nam S, Kim HS (2017) Influence of high-pressure torsion and hot rolling on the microstructure and mechanical properties of aluminum–fullerene composites. J Mater Sci 52:11988–12000. https://doi.org/10.1007/s10853-017-1230-3

[5] Wei L, Han B, Ye F, Ditta A, Wu S (2020) Influencing mechanisms of heat treatments on microstructure and comprehensive properties of Al–Zn–Mg–Cu alloy formed by spray forming. J Mater Res Technol 9(3):6850–6858

[6] Zhang C, Yadav V, Moelans N, Jensen D, Yu T (2022) The effect of voids on boundary migration during recrystallization in additive manufactured samples-a phase field study. Scr Mater 214:114675

[7] Liang S, Wei C, Ke C (2021) Effect of anisotropy in thermal conductivity on grain boundary migration under temperature gradient - a phase field study. Mater Lett 303:130517

[8] Jin Y, Bozzolo N, Rollett AD, Bernacki M (2015) 2D finite element modeling of misorientation dependent anisotropic grain growth in polycrystalline materials: level set versus multi-phase-field method. Comput Mater Sci 104:108–123

[9] Steiner MA, Mccabe RJ, Garlea E, Steiner M (2017) Monte Carlo modeling of recrystallization processes in alpha-uranium. J Nucl Mater 492:74–87

[10] Schwen D, Schunert S, Jokisaari A (2021) Evolution of microstructures in radiation fields using a coupled binary-collision Monte Carlo phase field approach. Comput Mater Sci 192:110321

[11] Salehi MS, Serajzadeh S (2012) Simulation of static recrystallization in non-isothermal annealing using a coupled cellular automata and finite element model. Comput Mater Sci 53:145–152

[12] Ach U (2021) Modeling of microstructure evolution during deformation processes by cellular automata-boundary conditions and space reorganization aspects. Materials 14:1377

[13] Teferra K, Rowenhorst DJ (2021) Optimizing the cellular automata finite element model for additive manufacturing to simulate large microstructures. Acta Mater 213:116930

[14] Li X, Ma W (2021) Molecular dynamics simulation and theoretical modeling of free surface effect on nanocrack initiation induced by grain boundary sliding in nanocrystalline materials. Mater Lett 304:130647

[15] Yang Q, Xue C, Chu Z, Li Y, Ma L, Gao H (2021) Molecular dynamics study on the relationship between phase transition mechanism and loading direction of AZ31. Sci Rep 11:17229

[16] Zhang H, Wang J, Chen Q, Shu D, Wang C, Chen G, Zhao Z (2019) Study of dynamic recrystallization behavior of T2 copper in hot working conditions by experiments and cellular automaton method. J Alloy Compd 784:1071–1083

[17] Zhang F, Liu D, Yang Y, Liu C, Zhang Z, Wang H, Wang J (2020) Investigation on the meta-dynamic recrystallization behavior of inconel 718 superalloy in the presence of δ phase through a modified cellular automaton model. J Alloy Compd 817:152773

[18] Lin YC, Liu Y, Chen M, Huang M, Ma X, Long Z (2016) Study of static recrystallization behavior in hot deformed Ni-

based superalloy using cellular automaton model. Mater Des 99:107–114

[19] Madej L, Sitko M, Radwanski K, Kuziak R (2016) Validation and predictions of coupled finite element and cellular automata model: influence of the degree of deformation on static recrystallization kinetics case study. Mater Chem Phys 179:282–294

[20] Chen F, Qi K, Cui Z, Lai X (2014) Modeling the dynamic recrystallization in austenitic stainless steel using cellular automaton method. Comput Mater Sci 83:331–340

[21] Bakhtiari M, Salehi MS (2018) Reconstruction of deformed microstructure using cellular automata method. Comput Mater Sci 149:1–13

[22] Timoshenkov A, Warczok P, Albu M, Klarner J, Kozeschink E, Bureau R, Sommitsch C (2014) Modelling the dynamic recrystallization in C-Mn micro-alloyed steel during thermomechanical treatment using cellular automata. Comput Mater Sci 94:85–94

[23] Jin Z, Liu J, Cui Z, Wei D (2010) Identification of nucleation parameter for cellular automaton model of dynamic recrystallization. Trans Nonferrous Met Soc 20:458–464

[24] Jin Z, Cui Z (2012) Investigation on dynamic recrystallization using a modified cellular automaton. Comput Mater Sci 63:249–255

[25] Madej L, Sitko M, Legwand A, Perzynski K, Michalik K (2018) Development and evaluation of data transfer protocols in the fully coupled random cellular automata finite element model of dynamic recrystallization. J Comput Sci 26:66–77

[26] Chen K, Tang J, Jiang F, Teng J, Zhang H (2019) The role of various Zr additions in static softening behavior of Al–Zn–Mg–Cu alloys during interval holding of double-stage hot deformation. J Alloy Compd 792:1112–1121

[27] Jiang F, Zurob HS, Purdy GR, Hui Z (2015) Static softening following multistage hot deformation of 7150 aluminum alloy: experiment and modeling. Mat Sci Eng A-Struct 648:164–177

[28] Pouraliakbar H, Pakbaz M, Firooz S, Jandaghi MR, Khalaj G (2016) Study on the dynamic and static softening phenomena in Al–6Mg alloy during two-stage deformation through interrupted hot compression test. Measurement 77:50–53

[29] Bo G, Jiang F, Su H, Wu L, Zhang H (2020) Static softening behavior and modeling of an Al–Cu–Mg–Zr alloy with various pre-precipitation microstructures during multistage hot deformation. Mat Sci Eng A-Struct 778:139094

[30] Zhang F, Liu D, Yang Y, Wang J, Zheng Y (2017) Study of factors affecting simulation of static recrystallization of Ni-based superalloy through cellular automaton model. Procedia Eng 207:2131–2136

[31] Sitko M, Chao Q, Wang J, Perzynski K, Madej L (2020) A parallel version of the cellular automata static recrystallization model dedicated for high performance computing platforms - development and verification. Comp Mater Sci 172:109283

[32] Zheng C, Xiao N, Li D (2008) Microstructure prediction of the austenite recrystallization during multi-pass steel strip hot rolling: a cellular automaton modeling. Comput Mater Sci 44:507–514

[33] Zhang T, Li L, Lu S, Zhang J, Gong H (2018) Comparisons of flow behavior characteristics and microstructure between asymmetrical shear rolling and symmetrical rolling by macro/micro coupling simulation. J Comput Sci 29:142–152

[34] Liu W, Chen X, Ahmad T, Zhou C, Xiao X, Wang H, Yang B (2022) Microstructures and mechanical properties of Cu–Ti alloys with ultrahigh strength and high ductility by thermo-mechanical treatment. Mat Sci Eng A-Struct 835:142672

[35] Yu X, Chen S, Wang L (2009) Simulation of recrystallization in cold worked stainless steel and its effect on chromium depletion by cellular automaton. Comput Mater Sci 46:66–72

[36] Zheng C, Raabe D (2013) Interaction between recrystallization and phase transformation during intercritical annealing in a cold-rolled dual-phase steel: a cellular automaton model. Acta Mater 61:5504–5517

[37] Madej L, Sieradzki L, Sitko M, Perzynski K, Radwanski K, Kuziak R (2013) Multi scale cellular automata and finite element based model for cold deformation and annealing of a ferritic–pearlitic microstructure. Comput Mater Sci 77:172–181

[38] He H, Yi Y, Huang S, Zhang Y (2019) An improved process for grain refinement of large 2219 Al alloy rings and its influence on mechanical properties. J Mater Sci Technol 35:55–63. https://doi.org/10.1016/j.jmst.2018.09.007

[39] Guo W, Yi Y, Huang S, He H, Fang J (2020) Effects of warm rolling deformation on the microstructure and ductility of large 2219 Al–Cu alloy rings. Met Mater Int 26:56–68

[40] Liu L, Wu Y, Ahmad S (2021) A novel simulation of continuous dynamic recrystallization process for 2219 aluminium alloy using cellular automata technique. Mat Sci Eng A-Struct 815:141256

[41] Oudin A, Barnett MR, Hodgson PD (2004) Grain size effect on the warm deformation behaviour of a Ti-IF steel. Mat Sci Eng A-Struct 367:282–294

[42] Yoshie A, Fujita T, Fujioka M (1996) Formulation of the decrease in dislocation density of deformed austenite due to static recovery and recrystallization. ISIJ Int 36:474–480

[43] Ding R, Guo ZX (2001) Coupled quantitative simulation of microstructural evolution and plastic flow during dynamic recrystallization. Acta Mater 49:3163–3175

[44] Ding R, Guo ZX (2002) Microstructural modelling of dynamic recrystallisation using an extended cellular automaton approach. Comput Mater Sci 23:209–218

Publisher's Note Springer Nature remains neutral with regard to jurisdictional claims in published maps and institutional affiliations.